Thermally Drawn Soft Dielectric Elastomer Actuator Fibers

Yuto Akimoto, Gildas Coativy, Jean-Yves Cavaillé, Jérôme Adrien, Eric Maire, Yuanyuan Guo

ACS OMEGA

Open Access

http://pubs.acs.org/journal/acsodf

Article

Thermally Drawn Soft Dielectric Elastomer Actuator Fibers

Yuto Akimoto, Gildas Coativy, Jean-Yves Cavaillé, Jérôme Adrien, Eric Maire, and Yuanyuan Guo*

Cite This: *ACS Omega* 2026, 11, 5716−5725

Read Online

ACCESS | Metrics & More | Article Recommendations | Supporting Information

ABSTRACT: The thermal drawing process, originally developed to fabricate silica-based optical fibers, has recently been adapted to produce polymer-based, multimaterial, and multifunctional fibers. Such fibers integrate electrodes, optical waveguides, microfluidic channels, and biosensors and are emerging as promising platforms for multimodal biointerfaces. Recently, actuation has been achieved within fibers by incorporating functional components such as shape-memory alloys (SMAs), magnetic composites, and tendon wires, expanding their applications to soft robotics and medical catheters. However, such actuator fibers often suffer from high stiffness, limited degrees of freedom, and complex actuation setups due to the use of rigid materials, such as SMA or magnetic setups, for field control. To overcome the limitations of existing thermally drawn fiber-based actuator systems, this study presents the development of all-polymer soft actuator fibers based on dielectric elastomers, designed to provide enhanced mechanical compliance and increased actuation freedom. A thermoplastic polyurethane (PU) elastomer was selected as the primary material due to its compatibility with the thermal drawing process and its electroactive response under applied electric fields. The resulting dielectric elastomer actuator (DEA) fibers exhibit intrinsic softness, with an overall Young's modulus of 37 MPa, enabling electrically controllable actuation modes with high freedom in bending, compression, and three-dimensional(3D) swirling motions. An estimated compression strain of 1.59% was achieved at a driving frequency of 1 Hz and an electrical field of 2.4 MV/m, which is consistent with literature-reported values. Furthermore, the fibers demonstrated excellent cyclic stability, maintaining a consistent actuation performance over 400 consecutive cycles. This approach provides a promising route toward flexible, scalable, and multifunctional actuator fibers for next-generation applications in soft robotics, biomedical devices, and wearable systems.

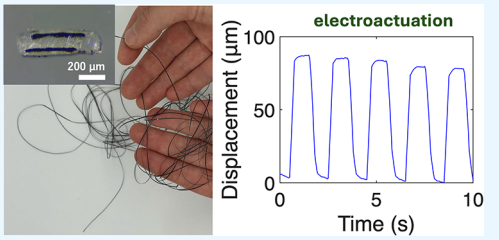

INTRODUCTION

Actuations are essential technologies in enabling motion and mechanical interaction in a wide range of systems, from industrial automation and soft robotics to biomedical devices.[1] In particular, soft actuators have gained increasing attention in recent years because of their intrinsic mechanical compliance, adaptability, and safety in interacting with biological tissues and delicate environments.[2] Among various mechanisms for achieving soft actuation, dielectric elastomer actuators (DEAs) have emerged as a promising class of materials, offering lightweight construction, significant strain response, and direct electrical control.[3,4] DEAs typically consist of a soft dielectric elastomer film sandwiched between compliant electrodes.[5−7] When a high electric field is applied to a dielectric elastomer actuator (DEA), the Maxwell stress (eq 1) compresses the dielectric layer, reducing its thickness while expanding its area, which induces mechanical deformation(eq 2).

$$p = \epsilon_0 \epsilon_r \left(\frac{V}{d}\right)^2 \tag{1}$$

$$\alpha = \frac{p}{E} \tag{2}$$

where p is the Maxwell stress (Pa), ϵ_0 is the vacuum permittivity (F/m), ϵ_r is the relative permittivity of the elastomer, V is the applied voltage (V), d is the thickness of the elastomer (m), α is the strain in the thickness direction, and E is Young's modulus (Pa)

Currently, most DEAs are fabricated primarily by planar methods, which involve sputtering metal, such as gold, or spin-coating stretchable electrode materials, such as CNTs, into dielectric elastomer films.[4,8,9] Recently, molding,[10] 3D printing,[11,12] and inkjet printing[13,14] have also been used to fabricate DEAs. However, these methods produce DEAs ranging from the centimeter to millimeter scale, making it challenging to scale them down for microscale applications.

Recently, the thermal drawing process, a scalable fabrication method for silica-based optical fibers, has evolved into a versatile platform for producing multifunctional and multimaterial fibers.[15,16] By drawing a macroscale preform composed of multiple functional components into fibers with its footprint on the microscales, the function and geometry as defined in the preform are conserved. A diverse array of

Received: September 15, 2025
Revised: November 13, 2025
Accepted: December 10, 2025
Published: January 20, 2026

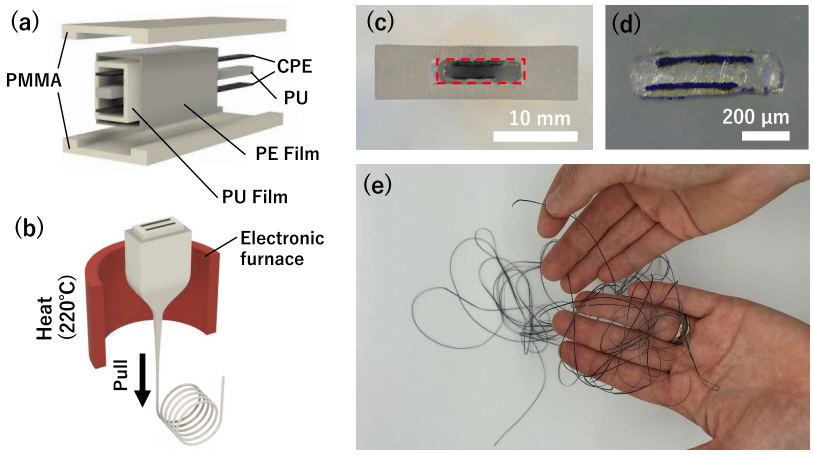

Figure 1. Soft DEA fiber fabrication process. (a) Preform structures. (b) Thermal drawing process to draw macroscopic preforms into fibers. (c) Cross-sectional image of the preform. (d) Thermally drawn soft DEA fibers after removing the PMMA cladding layer. (e) Image of decades of meter-long DEA fibers after removing the PMMA cladding layer.

functions, such as electrodes, optical waveguides, microfluidic channels, and sensing elements, can be readily integrated into a flexible fiber. These thermally drawn fibers have been demonstrated for promising applications in biosensing,[17] neural interfaces,[15,16] and wearable systems.[18]

Recent efforts have been made to expand the functionality of thermally drawn fibers to include actuation, enabling motion and shape change. This has primarily been achieved by incorporating shape-memory alloys (SMAs),[19] shape-memory polymers (SMPs),[20,21] magnetic composites,[22,23] or tendon wires[24] into the fiber structure. Although these approaches demonstrate potential for applications in catheter steering, soft manipulators, and haptic interfaces, they suffer from several limitations. The reliance on rigid materials, such as SMA or tendon metal wires, results in high mechanical stiffness, which limits flexibility and adaptability. In addition, these systems often involve complex actuation mechanisms, such as Joule heating-induced phase change,[19] thermal expansion,[25] and external magnetic fields,[22] which limit their practical applications.

To overcome these challenges, we developed all-polymer soft actuator fibers based on dielectric elastomers. By employing the thermal drawing technique and selecting thermoplastic polyurethane (PU) as the active material, owing to its compatibility with thermal drawing, electro-actuation capability,[8,26−28] and relatively high dielectric constant (2−8),[29] we realized soft fiber-based DEA actuators with intrinsic mechanical compliance. The resulting fibers exhibit a Young's modulus of 37 MPa and enable electrically controllable actuation with high degrees of freedom, including bending, compression, and 3Dswirling motions. A representative compression strain of 1.59% was achieved at a driving frequency of 1 Hz and an electrical field of 2.4 MV/m. Additionally, in both bending and compression configurations, the displacement amplitude decreased as the frequency increased, consistent with viscoelastic damping within the PU and encapsulation layers. Furthermore, the fibers demonstrated excellent cyclic stability, maintaining consistent actuation performance over 400 consecutive cycles. These thermally drawn soft DEA fibers could open up new possibilities for scalable, flexible, and integrable actuation systems, with potential applications in soft robotics,[7,30] wearable devices, and biomedical technologies.[5]

EXPERIMENTAL METHODS

Materials and Equipment

Materials. The primary material used is polyurethane (Lubrizol ESTANE 58125 NAT 055) in granular form. Carbon-based polyethylene (CPE) film with a thickness of 50 μm (No. ZC-85) was obtained from Engineer Inc.. Additionally, polyurethane (PU TG88-I) and polyethylene films, each with a thickness of 50 μm, were purchased from Takeda Sanygo and AS ONE Corp., respectively. AS ONE Corp. also supplied poly(methyl methacrylate) (PMMA) in a rectangular block with dimensions of 4 × 24 × 180 mm^3. All materials were stored under vacuum conditions to prevent moisture absorption. This precaution is essential because moisture can impede fiber fabrication, such as nonuniform deformation, especially during the drawing process.

Equipment. All cross-sectional observations and analyses were performed using a stereomicroscope (Stemi 305, ZEISS) equipped with Labscope software. For detailed microstructural analysis, a scanning electron microscope (SEM, HITACHI) and an X-ray tomography system (Easytom Nano, Rx Solutions) were utilized. Young's modulus was measured using a tensile testing machine (MCT-2150, AND Corp.). Fiber fabrication was conducted by using a customized thermal drawing system. For electrical characterization, a high-voltage amplifier (HVA 4321, NF Corp.) and a digital function generator (DF 1906, NF Corp.) were used. Displacement measurements were carried out using a laser displacement sensor (LK-GD500, KEYENCE).

Fiber Fabrication

To make PU plates, the PU granules (Lubrizol ESTANE 58125 NAT 055) were thermally pressed at 180 °C for 10 min to form plates with dimensions of 1 mm × 24 mm × 200 mm. These plates were then cut into narrower strips measuring 1 × 8 × 200 mm^3. A sandwich structure was constructed by placing a CPE film (thickness: 50 μm) on both the top and bottom surfaces of the PU plate. Subsequently, the PU−CPE assembly was wrapped sequentially with the PU film and the PE film, followed by heat pressing under vacuum conditions at 180 °C for 1 min. After heat pressing, the structure was clamped using PMMA blocks (dimensions: 4 mm × 24 mm × 180 mm) that were premachined with a central groove of 1.5 mm × 8 mm × 180 mm using a CNC milling machine from Seaforce Co. The

https://doi.org/10.1021/acsomega.5c09586
ACS Omega 2026, 11, 5716−5725

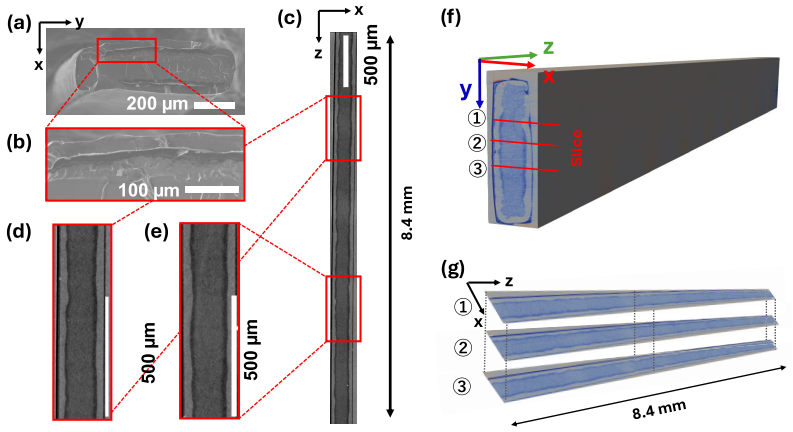

Figure 2. Structural characterization of the soft DEA fibers via SEM and X-ray tomography. (a) SEM image of the DEA fiber cross sections. (b) Close-up SEM image of the carbon electrode with the PU layer, showing strong adhesion. (c) One representative frame of the 3D scan of X-ray tomography along the fiber longitudinal direction showing the continuous structures with close-ups shown in (d) and (e). (f) 3D scan of the X-ray tomography along the fiber longitudinal direction, with representative three slices shown in (g).

final assembly was then thermally pressed again at 180 °C for 10 min. The PE film served as a separator layer, facilitating the delamination of the PMMA and PU components after the thermal drawing process (Figure 1(a)).

Additionally, to reduce the weight and thickness of the additional encapsulation layer of the PU-based DEA fiber, we also fabricated a thin-shell version via wrapping the sandwich structure with only PE layers; no additional PU films were used (Supporting Figure S8).

Due to the high melt flow characteristics of PU, thermal drawing of solely PU-based preforms remains challenging. Therefore, the use of rigid PMMA blocks provided mechanical guidance and structural stability during the drawing process, enabling successful fiber formation.

The two-step thermal pressing process was designed to remove trapped air bubbles within the preform, which can cause defects during the fiber drawing process. The first heat pressing step was especially critical for degassing and minimizing bubble formation inside the preform and the PU plate, which serves as the core material for dielectric actuation later. The fabricated preform was drawn into fibers using a thermal drawing tower capable of precise temperature and tension control (Figure 1(b)). The preform was heated to 220−230 °C to achieve the appropriate flow characteristics for drawing. At the beginning of the drawing process, a tension of 80*g* was applied by using a weight to initiate the drawing for the bait-off process. Under these conditions, fibers with lengths of several decades of meters were successfully obtained (Figure 1(e)), and their cross-sectional structure was preserved along the length (Figure 1(c,d)).

Additionally, to reduce the overall weight and thickness of the encapsulation layer in the PU-based DEA fiber, a thin-shell version was fabricated by wrapping the sandwich structure with only PE layers without using additional PU films. This modification can reduce the overall stiffness and viscoelastic damping of the fiber, resulting in enhanced deformation under an applied electric field. However, we also tried to increase the sandwich electrode area, which leads to higher leakage risks, likely due to the reduced insulation thickness at the corners and greater susceptibility to dielectric breakdown along the electrode interfaces (Supporting Figure S8).

SEM Observation

The fibers produced via the thermal drawing process were cut into small segments of approximately 5 cm length using a razor blade. PU and PMMA components had already been delaminated. To observe the composite material's internal structure, a clean cross-sectional surface needed to be exposed. For this purpose, the fiber segments were immersed in liquid nitrogen to induce a brittle freezing fracture. While in the frozen state, mechanical force was applied to both ends of the sample using a custom jig, causing the fiber to fracture and cleanly expose the internal cross section. This liquid nitrogen fracture method enabled detailed observation of the internal morphology using SEM while preserving the sample's structural integrity (Figure 2(a,b)).

X-ray Tomography Observation

X-ray tomography measurements were conducted using a laboratory X-ray source at high resolution, with a 0.9 μm^3 voxel size. This tomograph is equipped with a LaB_6 emission tip for the X-ray source, which ensures that the actual spot size is physically smaller than 0.9 μm. The resolution is then not altered by geometric blur. The Hammamatsu X-ray source was operated at a voltage of 50 kV to allow good contrast with the absorbent materials. The detector was a CCD camera from Hamamatsu with a pixel size of 11.8 μm. A series of nine scans along the height of the sample were performed to image the 8.4 mm section (Figure 2(c−g)). Each scan consisted of 800 projections over a 360-degree rotation. The exposure time for a single radiograph was 0.6 s. An average of five images was taken for each angle to reduce noise. These parameters resulted in a total measurement period of about 6 h for the full length of the sample being analyzed. All of the data were reconstructed by a filtered back-projection Feldkamp algorithm. Fibers with intact PU and PMMA components were used. Delaminated fibers were too soft and could not be fixed in a straight configuration, making them unsuitable for high-resolution tomographic imaging. Similar to the SEM preparation, the fiber was cut into approximately 5 cm segments by using a razor blade. The lower end of each segment was then fixed securely to maintain alignment during scanning. The tomography was performed with the fiber in a stable vertical orientation to minimize distortion and ensure accurate internal structural imaging.

https://doi.org/10.1021/acsomega.5c09586
ACS Omega 2026, 11, 5716−5725

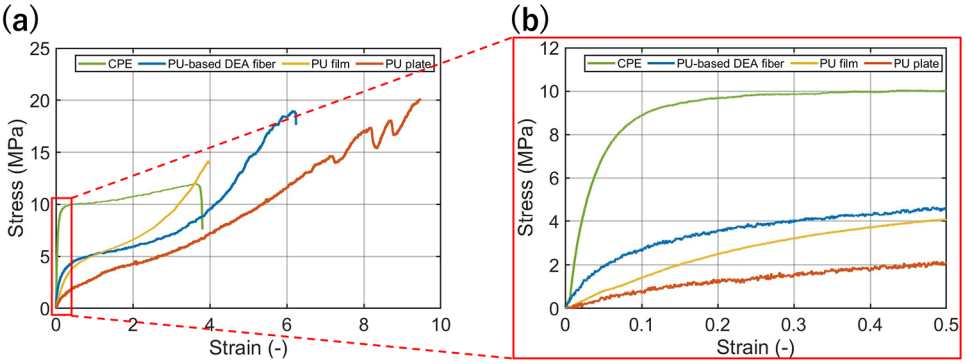

Figure 3. Mechanical characterization of the DEA fibers with their constituent materials. (a) Strain−stress characterization of all of the materials and fiber units until they fracture. (b) Close-up strain range, which contains the elastic region from which the Young modulus can be determined.

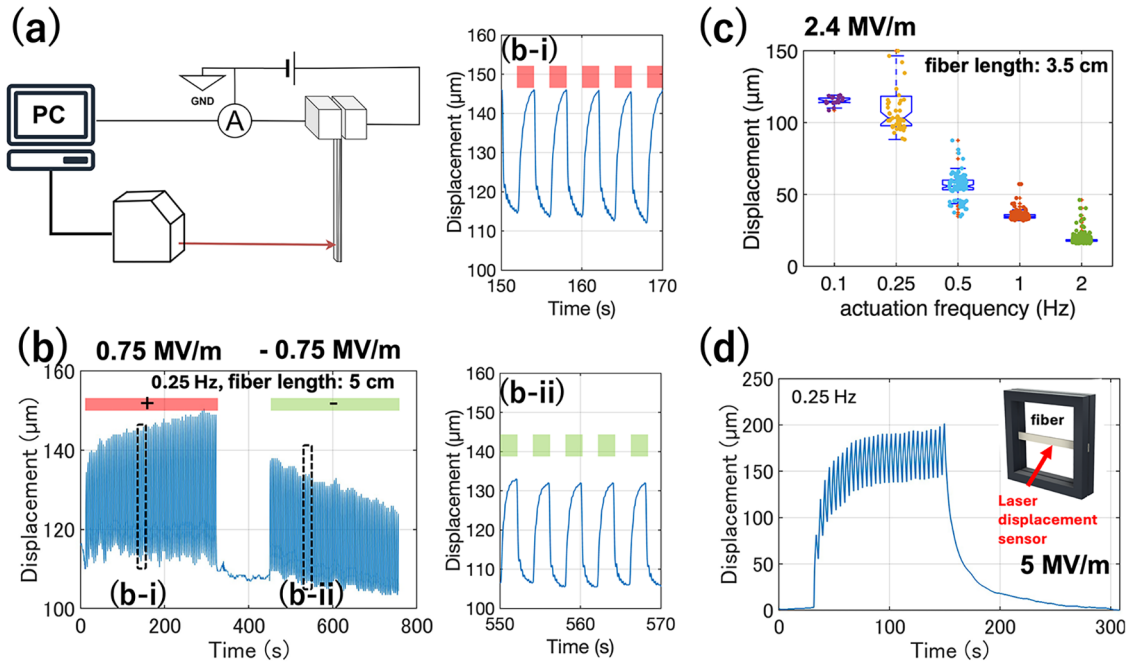

Figure 4. Actuation characterization of the PU-based DEA fibers. (a) Experimental setup to characterize the bending actuation of the fiber samples. (b) DEA actuation behaviors of the fiber sample. The fibers show DEA actuation behaviors regardless of the polarity of the applied electrical field, with a zoom-in of the actuation behavior under a positive electric field in (b-i) and a zoom-in of the actuation behavior under a reversed (negative) electric field in (b-ii). (c) Frequency dependency of the bending actuation behaviors. (d) Actuation behaviors of the DEA fiber with both terminals fixed; length: 3 cm.

Tensile Test

Tensile tests were performed on each fiber constituent material, including the DEA fiber based on PU (PU-based DEA fiber), the electrode (CPE), the PU actuation layer (PU plate), and the encapsulating PU film (PU film), to evaluate their respective Young's modulus (Figure 3). The samples were cut to a length of 3 cm and tested using a universal test machine. The tests were performed at a constant crosshead speed of 10 mm/min, continuing until fracture. The stress−strain curves were recorded for each material, and Young's modulus was determined from the slope of the initial linear region of the stress−strain curve.

Fabrication and Configuration of Bending-Type and Fixed-End DEA Fiber Actuators

For bending-type actuator devices, PU-based DEA fiber samples with lengths of 5, 3.5, and 1.5 cm were prepared. Electrical connections were formed at one end of each fiber. A small window was created on one side of the sandwich structure using a razor blade to expose the underlying carbon−polyethylene (CPE) electrode layer, which served as the contact point. Silver paste was applied to the exposed area to ensure a stable and low-resistance electrical connection. The same procedure was repeated on the opposite side of the fiber at the same terminal. The exposed ends were then sandwiched between aluminum-film-lined plastic substrates, and the electrical contacts were mechanically secured with clips.

In addition to exhibiting bending actuation, the soft PU-based DEA fibers can be thermally reshaped into 3D architectures, such as spiral configurations, to achieve swirling or helical actuation motions.

For the configurable devices with both fiber ends fixed, a 3 cm-long sample was prepared, and electrical connections were established at both terminals of the fiber. The same electrode exposure and contact procedures were employed to connect the devices to the external power supply system.

https://doi.org/10.1021/acsomega.5c09586
ACS Omega 2026, 11, 5716−5725

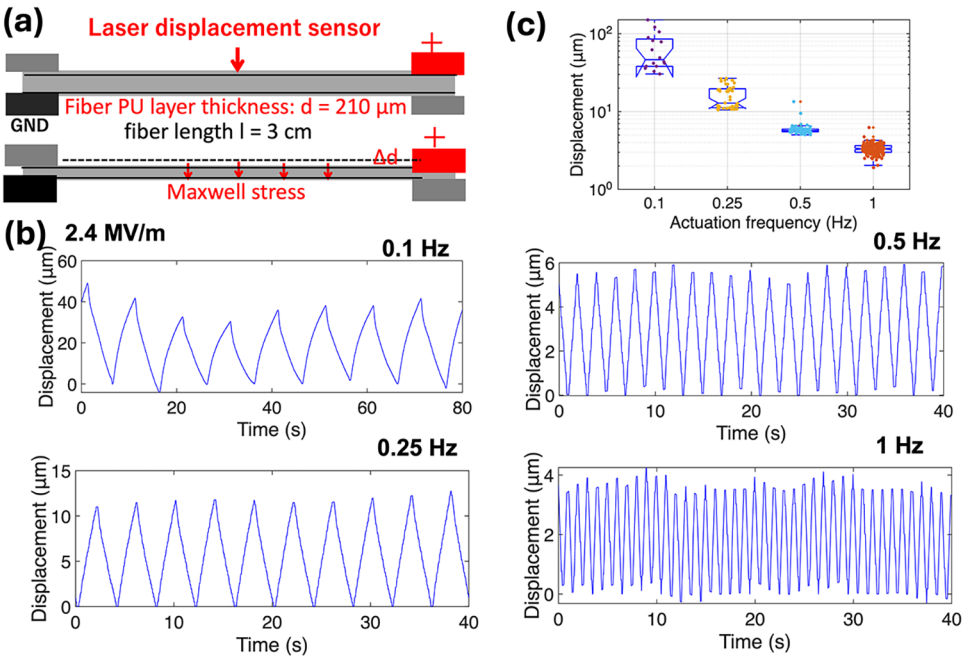

Figure 5. Characterization of thickness-direction compression strain in PU-based DEA fibers under a two-end fixed configuration. (a) Schematic illustration of Maxwell stress-induced compression in the dielectric layer of the PU-based DEA fiber. (b) Electrostriction-driven actuation responses of the fiber measured at various actuation frequencies. (c) Frequency-dependent displacement amplitude.

Characterization of Actuation Performances of the DEA Fibers

Evaluation of Electrostriction-Driven Actuation under Applied AC Pulsed Voltage. The electrostriction-driven actuation of the fabricated DEA fiber devices was evaluated by using a power supply and amplifier system capable of delivering up to 10 kV. During testing, the fibers were suspended vertically, with the positive and negative terminals connected to the aluminum-film-covered plastic electrodes at each end of the fiber (Figure 4(a)).

A laser displacement sensor was aligned to the bottom tip of the suspended fiber to measure the axial displacement. The input voltage was applied in the form of a pulsed waveform, with the voltage amplitude varying from 75 V to 1 kV and the driving frequency adjusted between 0.1 and 2 Hz (Figure 4(b,c)).

For configurable devices with both ends fixed, a customized 3D printed frame was used to secure the fiber devices (a length of 3 cm) and form the connections. A power supply (500 V, 0.25 Hz) was provided from both ends of the fiber, and its actuation behavior was recorded both via laser displacement sensors (Figure 4(d)). Simultaneously, a high-resolution camera was used to observe the device's motion during actuation, allowing for a correlation between the displacement test and actual actuation behavior (Supporting movie 1).

Additionally, as both terminals of the fiber were fixed, the observed oscillatory actuation behavior primarily originated from the compression of the dielectric layer within the fiber (Figure 5(a)), whereas the slow variation in bending behavior (Figure 4(d)) indicated the presence of a slower response component, which can be attributed to the charge mobility within the PU layer. After correcting the DC baseline change, the corresponding compression strain in the thickness direction was calculated as $\varepsilon = \frac{\Delta d}{d}$. We further investigated the displacement and compression strain dependence of our DEA fiber with its two terminals fixed.

Ionic-Conduction-Driven Actuation under Applied DC Voltage. To investigate baseline drifting behavior and elucidate the role of ionic conduction in the actuation mechanism, bending-type PU-based DEA fiber devices were tested under a DC electric field. Prior to measurement, the fibers were soaked in a 5.7 M sodium acetate solution for 3 h to enhance ionic conductivity. A DC voltage step was applied to a 3 cm-long sample using a function generator (Keysight 33220A) in combination with a high-voltage amplifier (TREK 609D-6). The current response was recorded with a current preamplifier (Stanford SR570), while the resulting mechanical displacement was measured using a laser displacement sensor (Keyence LK-H052 head with LK-G5001PV controller) (Supporting Figure S7).

Electrical Impedance Characterization of DEA Fiber Devices

To better understand its ionic conduction and dielectric behaviors, the electrical impedance of the DEA fiber devices was characterized by using electrochemical impedance spectroscopy (EIS) mode on a potentiostat (Gamry Interface 1010E). Measurements were performed over the frequency range of 0.01−10 Hz with a sinusoidal excitation voltage of 5 mV (rms). The lower frequency limit was adjusted to account for the instrument's precision and the maximum measurable impedance at very low frequencies.

RESULTS AND DISCUSSION

Structural Characterization of PU-Based DEA Fibers

Cross-sectional observations using an optical microscope revealed a clearly defined interface between the PU and CPE layers, indicating that the multilayer structure was well preserved after fabrication (Figures 1(d) and S3). SEM analysis further confirmed that the interfaces between the

https://doi.org/10.1021/acsomega.5c09586
ACS Omega 2026, 11, 5716−5725

electrode and dielectric PU elastomer remained firmly intact after thermal drawing with no signs of delamination (Figure 2(a,b)). This observation suggests strong adhesion between the constituent materials despite differences in their thermomechanical behaviors and chemical properties. The strong adhesion between the electrode and the dielectric elastomer plays an important role in DEA fiber actuation behaviors. In addition to the two-dimensional (2D) structural analysis, we also performed X-ray computed tomography (CT) to reveal the 3D structure of the DEA fiber in a nondestructive manner (Figure 2(c)). CT scan demonstrated that the sandwich structure of the DEA fiber remained continuous, especially CPE was embedded continuously throughout the fiber without interruption in the vertical (z-axis) direction, as illustrated in Figure 2(c−g). This confirms that electrical connectivity is maintained along the entire length of the actuator component, allowing voltage applications across the entire fiber structure. In addition, these images clearly show that the distance between the electrodes is approximately 100−200 μm, which is in the range suitable for electroactuation. They also show that the fibers are not perfectly symmetrical, which can cause the dielectric elastomers to bend under the effect of an electric field, even in the case of electrostriction.[31]

Mechanical Characterization of DEA Fibers

The tensile test was performed for each constituent material and for the entire PU-based DEA fiber (PU-based DEA fiber). The tensile testing machine applies a tensile force to the fiber, increasing it gradually until the fiber fractures. From the obtained strain−stress curve (Figure 3(a)), we identified the elastic region where we calculated the Young's modulus. As shown in Figure 3(b), the CPE exhibited a significantly higher Young's modulus of 115 MPa (strain 0−0.05) compared to the other individual materials with a PU actuation layer of 8 MPa (strain 0−0.1) and a PU encapsulation layer of 13 MPa (strain 0−0.15). Additionally, the overall modulus of the PU-based DEA fiber itself was measured to be 37 MPa (strain 0−0.05), indicating that the soft and flexible nature of the PU layer significantly contributed to the response. This value is substantially lower than that of typical thermoplastics, confirming that the fabricated DEA fiber possesses a high degree of flexibility, which is essential for actuator applications. However, the major limiting factor here for PU-based electroaction is the electrode materials based on CPE. The CPEs have a significantly higher Young's modulus than the PU actuation layer and limited elastic regions, which can significantly reduce the actuation strain of the actuator.

Characterization of Electrostriction Actuation of DEA Fibers

We first investigated the bending behaviors of DEA fiber actuation by fixing one end of the fibers (Figure 4(a)). When an AC voltage was applied to the device using an amplifier, the fiber exhibited alternating displacement at its lower end. The displacement was quantified using a laser displacement sensor positioned at the tip of the suspended fiber. A pulsed voltage waveform was applied while systematically varying the applied voltage and frequency. As observed across all displacement graphs, the DEA fiber's actuation consistently responded to the voltage input, showing synchronous increase and decrease in displacement corresponding to its driving frequency. In Figure 4(b), a low-frequency signal (0.25 Hz) was applied with alternating positive and negative electrical fields (0.75 MV/m). Actuation was clearly observed, even under such a low field strength in driving the DEA. Notably, despite the reversal of the applied field polarity, the displacement direction remained unchanged. A magnified view of the actuation behavior is provided in Figure 4(b-i,ii). This behavior indicates that the actuation mechanism in PU, characterized by response times on the order of seconds or less, is primarily governed by electrostriction, a phenomenon commonly observed in dielectric polymers and known to induce bending in asymmetric structures.[31] The origin of the low-field actuation observed here remains unclear. We hypothesize that it may be related to impurities present in industrial-grade PU, which could alter its relative permittivity ϵ_r. Additionally, it could also be related to the alteration of Young's modulus and resistivity of the CPE electrodes after thermal drawing. These possibilities will require further investigation. For validation reference, electrostriction-based actuation has also been observed in other DEA fiber devices, showing repeatability (Supporting Figures S4 and S5, which were driven by electrical fields of 5 and 8.3 MV/m, respectively).

To investigate frequency dependence, the driving electrical field was kept constant at 2.4 MV/m and only the frequency was varied, as shown in Figure 4(c). A significant reduction in displacement amplitude was observed with an increase in frequency. To be noted, the DC baseline offset has been corrected to reveal the frequency-dependent actuation behaviors. Representative displacement traces under different frequencies are presented in Supporting Figure S9. This frequency-dependent behavior could be primarily attributed to the viscoelastic behaviors of elastic fibers. An additional reason could be the presence of impurities and their drift under the effect of the electric field, causing local stress.[8,26] When the frequency increases, the actuation time becomes insufficient for the DEA fiber to reach its full deformation, thereby reducing the overall displacement amplitude.

These results collectively confirm that the actuation of the DEA fiber in AC voltage is primarily driven by dielectric effects in PU (at short time scales), modulated (at longer time scales on the order of 10 100 s) by the material's inherent viscoelasticity and the input signal conditions or by the presence of ionic impurities and their gradual drift at the origin of local stress.[8,26] In addition to the bending type of actuation, DEA fibers can be thermally reformed into different 3D shapes. For example, the spiral shape of the DEA fiber can be easily formed by thermal treatment, and it can produce rotational motions in response to voltage conditions of 500 V and 1 Hz (Supporting movie 2).

In Figure 4(d), both DEA fibers' terminals were fixed, and the electrical field was supplied from both ends. The displacement was measured at the center point of the fiber by the laser displacement meter, and the overall actuation was also recorded via camera (Supporting movie 1). In addition to the oscillatory displacement of 50 μm under an AC voltage, a slow, continuous increase of up to 200 μm in the positive direction was recorded. Upon stopping the voltage input, the displacement gradually returned to the original position. This relaxation behavior also suggests the presence of a secondary, slower response, likely attributable to impurity charge mobility within the PU, superimposed on the fast electrostrictive response. The partial contribution of impurity charges within the PU layer will be investigated using electrical impedance spectroscopy, as well as displacement driven by a DC field; the results of which are discussed in a later section.

https://doi.org/10.1021/acsomega.5c09586
ACS Omega 2026, 11, 5716−5725

Characterization of Compression Strain of DEA Fibers

We then focused on analyzing the compression strain in the thickness direction of PU-based DEA fibers under the two-end-fixed configuration (Figure 5). After the baseline drift was corrected, mainly attributed to impurity charge migration, as shown in Figure 4(d), the net electrostrictive deformation was analyzed at higher frequencies. The schematic in Figure 5(a) illustrates the Maxwell-stress-induced compression of the dielectric layer, resulting in a reduction of the in-fiber PU layer thickness (d) upon application of the electric field. Figure 5(b) presents representative actuation waveforms of the fibers subjected to pulsed driving voltages at different frequencies (0.1, 0.25, 0.5, and 1 Hz). The displacement amplitude decreased with increasing frequency, reflecting the viscoelastic relaxation behavior of the PU dielectric, encapsulation materials, electrode compliance, and impurities within the PU. Although the DC baseline shift has been corrected, the displacement at lower frequencies includes significant contributions from bending deformation induced by ionic migration. To ensure that the reported value predominantly reflects through-thickness electrostrictive compression, we therefore consider the actuation data with frequencies of 1 Hz, yielding a compression strain, calculated as

$$\varepsilon = \frac{\Delta d}{d}$$

of 1.59% at the electrical field of 2.4 MV/m, as the representative measure of the intrinsic electromechanical performance of the PU-based DEA fibers. It is also consistent with the classic work reported by Hirai et al.,[29] who studied the actuation strain in the range of 0.01−1.34% of PU with different chemical structures at 0.4 MV/m, and other review literature values of less than 5%.[7]

Characterization of Electrical Impedance and Cyclic Stability of PU-Based DEA Fibers

As the electromechanical response of the PU-based DEA fibers involves both ionic-conduction-driven actuation and dielectric-polarization-driven electrostriction, we investigated their electrical impedance characteristics to elucidate these underlying mechanisms (Figure 6(a)). The frequency-dependent impedance provides crucial insight into the charge transport and polarization dynamics within the dielectric layer, which directly influence the overall actuation performance. At high frequencies, the response is dominated by dielectric polarization, where the dipoles in the PU matrix align with the alternating electric field. In contrast, at lower frequencies, ionic migration and interfacial polarization processes become more pronounced, leading to increased leakage current and baseline drift during actuation.

From the impedance measurements, the cutoff frequency was determined to be 0.07 Hz, which represents the transition between the fast dielectric and slow ionic regimes. To further correlate the electrical and mechanical dynamics, we analyzed the temporal actuation response of the PU-based DEA fibers (Figures 6(b) and S6). The measured rise time of approximately 0.25 s, which is longer than the time response (ms) expected from the electrostriction actuation, indicates that the actuation speed is primarily limited by the viscoelastic response of the PU dielectric and the surrounding encapsulation layers, as well as potentially by the impurities present within the PU layers. This temporal behavior reflects the intrinsic electromechanical dynamics of the fiber, where

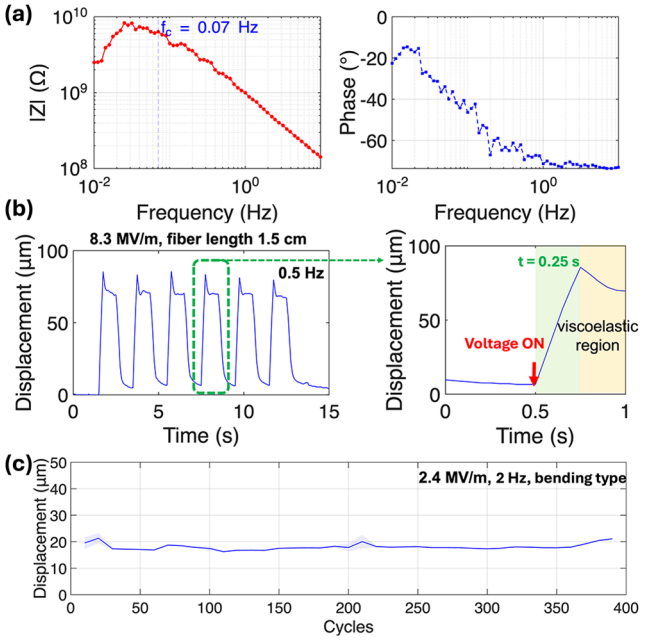

Figure 6. Characterization of electrical impedance and cyclic stability of actuation in PU-based DEA fibers. (a) Electrical impedance spectrum of the PU-based DEA fiber, showing a cutoff frequency of 0.07 Hz. Above this frequency, the fiber response is dominated by dielectric polarization, whereas below this frequency, ionic conduction becomes the dominant mechanism. The time constant of 2.3 s was calculated from the cutoff frequency, which represents a characteristic time of ion mobilities. (b) Temporal response of the PU-based DEA fiber in (a), demonstrating electrostriction-driven actuation accompanied by viscoelastic damping. The measured rise time of approximately 0.25 s corresponds to the time required to reach the maximum displacement induced by electrostriction and is significantly shorter than the time constant estimated from the cutoff frequency, indicating that the electrostriction is a much faster response compared to the ion-migration event. (c) Cyclic stability of actuation over 400 cycles; the shaded regions represent the average displacement over ten cycles with the corresponding standard deviation (fiber length: 3.5 cm).

rapid electrostriction is coupled with slower viscoelastic effects and an impurity-charged ion effect.

In addition, viscoelastic damping was observed following the electrostriction response. Such damping behavior can be mitigated by reducing the thickness of the encapsulation layers, employing more compliant electrode materials, and reducing the length of actuating fibers, thereby enhancing actuation efficiency. The electrical impedance analysis and temporal actuation response of the thin-shell PU-based DEA fiber are given in Supporting Figures S10 and S11. These findings collectively provide a foundation for understanding dynamic electromechanical coupling in PU-based DEA fibers.

Furthermore, we evaluated the cyclic stability of the PU-based DEA fibers under repeated operation. In a representative case of a bending-type actuator driven at 2 Hz, no significant degradation in actuation amplitude was observed after 400 consecutive cycles, demonstrating the mechanical and electrical durability of the fibers during a relatively extended use (Figures 6(c) and S12).

https://doi.org/10.1021/acsomega.5c09586
ACS Omega 2026, 11, 5716−5725

Investigation of Ion-Conduction-Induced Actuation in PU-Based DEA Fibers

To study the impurity charge-mobility-induced actuation, we also characterized the DC voltage response of the DEA fiber doped with sodium acetate. Displacement was quantitatively measured with a laser displacement sensor positioned at the tip of the vertically suspended fiber. As charge mobilities are associated with actuation, in addition to displacement, electrical current was simultaneously monitored during the application of a DC voltage, which is related to the charge mobilities (Supporting Figure S7). In Figure S7(a), both positive and negative voltages were applied to the PU-based DEA fibers. When a positive voltage was applied, the initial current exhibited capacitive charging behavior, characterized by a peak at the onset of voltage application and a gradual decrease over time, which is attributed to the movement of mobile charges in response to the applied electric field. Correspondingly, the displacement increased in the positive direction. A similar behavior in current was observed under the reversed polarity of the voltage, indicating symmetric response characteristics of the current to the electric field. However, the displacement exhibited a slow, gradual increase in the positive direction, and then it reversed its direction over time (as observed by Watanabe et al.[32]); the current asymptotically approached a small steady-state value. These observations suggest that the actuation is primarily driven by impurity-charged ion mobility, which is a relatively slow response within the PU layer, rather than by rapid dielectric responses. Also, the current response to applied voltages exhibits exponential decay, consistent with the behavior of a capacitive system. This indicates that the PU functions similarly to a dielectric material in a capacitor, where charge redistribution occurs in response to an electric field. In Figure S7(b), a stepwise increase in the applied positive DC voltage was performed. Despite some fluctuations in the measured current due to equipment settings, the overall behavior mirrored that in Figure S7(a): the current initially peaked and then decreased, while the displacement increased proportionally with the applied voltage. This suggests that charge movements within the PU primarily cause the displacement observed under a DC voltage. The mechanisms of DC-based actuation based on charge mobilities within the PU layer are shown in Supporting Figure S2.

CONCLUSIONS

In this work, we have successfully fabricated meter-long polyurethane (PU)-based dielectric elastomer actuator (DEA) fibers with continuous internal architectures through a thermal drawing process. To the best of our knowledge, this is the first demonstration of fiber actuation using thermoplastic PU as a dielectric polymer, marking a key step toward scalable soft actuator fibers. The fabricated PU-based DEA fibers exhibit robust adhesion between the electrodes and PU dielectric layers, which is essential for stable electromechanical coupling and reliable actuation under applied electric fields. The internal structure and material integrity were verified through non-destructive X-ray tomography, which revealed continuous and defect-free electrode and PU layers along the entire fiber length, confirming the structural fidelity of the thermally drawn fibers.

Functionally, the fibers exhibited electrostriction-driven actuation under AC electric fields, achieving multimodal deformation that included bending, compression, and 3D swirling motions, thereby demonstrating a high degree of actuation freedom. The representative compression strain reached 1.59% at 1 Hz and was driven at an electrical field of 2.4 MV/m. The overall displacement amplitude decreases at higher frequencies primarily due to the viscoelastic damping of the PU dielectric and encapsulation layers. In addition, DC-induced offset displacements were observed, which were analyzed through impedance spectroscopy to distinguish between fast dielectric polarization and slower charge-mobility-driven mechanisms. Additionally, the detailed charge-mobility-driven actuation in DC mode was also investigated by applying constant voltages.

Mechanically, the current carbon−polyethylene (CPE) electrodes, while compatible with thermal drawing, were identified as the primary limiting factor in overall actuation performance. The CPE exhibits a relatively high modulus and a narrow elastic region, leading to plastic deformation that can contribute to baseline shifts during cyclic actuation. Future optimization will focus on incorporating more compliant and stretchable electrode materials to enhance the electro-mechanical efficiency. Furthermore, the present study utilized industrial-grade PU for cost-effective fabrication; however, its mixed electrostriction and charge-mobility behavior suggests that future work using high-purity or custom-synthesized PU formulations could help decouple these mechanisms and improve actuation fidelity.

The developed DEA fibers are inherently flexible and reconfigurable, enabling postprocessing into complex 3D geometries. For instance, spiral-shaped DEA fibers can produce rotational or swirling motions, and woven arrangements can generate patterned two- or 3D textile-based actuations. These unique capabilities position the PU-based DEA fibers as versatile and scalable platforms for next-generation soft robotic systems, biomedical devices, and adaptive wearable technologies.

ASSOCIATED CONTENT

Supporting Information

The Supporting Information is available free of charge at https://pubs.acs.org/doi/10.1021/acsomega.5c09586.

Schematic of a dielectric elastomer under Maxwell stress when subjected to a high electric field; schematic of charge-mobility-induced fiber displacement driven by a DC-based electrical field; and optical microscopy images of fiber cross sections obtained at different longitudinal positions; Frequency-dependent actuation behavior of a representative PU-based DEA fiber; Representative PU-based DEA fiber showing its actuation behavior under different driving frequencies; the DC baseline shift has been corrected; Temporal response of the electro-actuation behavior of the PU-based DEA fiber; The detailed investigation of the bending induced by the DC electrical field; Development of the thin-shell PU-based DEA fiber fabricated in this study; Frequency dependence of the electrostriction-driven actuation behavior of the thin-shell PU-based DEA fiber driven under pulsed voltage; Temporal response of the electroactuation behavior of the thin-shell PU-based DEA fiber; Frequency-dependent impedance behavior of the thin-shell PU-based DEA fiber; Cyclic stability of electro-striction-driven actuation in PU-based DEA fibers (PDF)

https://doi.org/10.1021/acsomega.5c09586
ACS Omega 2026, 11, 5716−5725

Displacement was measured at the center point of the fiber by the laser displacement meter (MP4)

Spiral shape of the DEA fiber can be easily formed by thermal treatment, and it can produce rotational motions in response to voltage conditions of 500 V and 1 Hz (MP4)

AUTHOR INFORMATION

Corresponding Author

Yuanyuan Guo − *Frontier Research Institute for Interdisciplinary Sciences (FRIS), Sendai, Miyagi 980-0845, Japan; Graduate School of Biomedical Engineering, Sendai, Miyagi 980-0845, Japan;* orcid.org/0000-0002-9618-7919; Email: yyuanguo@fris.tohoku.ac.jp

Authors

Yuto Akimoto − *Department of Mechanical and Aerospace Engineering, School of Engineering, Tohoku University, Sendai, Miyagi 980-8579, Japan; Frontier Research Institute for Interdisciplinary Sciences (FRIS), Sendai, Miyagi 980-0845, Japan*

Gildas Coativy − *LGEF EA682, INSA Lyon, 69621 Villeurbanne, France*

Jean-Yves Cavaillé − *ELyTMaX IRL3757, CNRS, INSA Lyon, 69621 Villeurbanne, France;* orcid.org/0000-0002-1714-2684

Jérôme Adrien − *MATEIS UMR CNRS 5510, INSA-Lyon, 69621 Villeurbanne, France*

Eric Maire − *MATEIS UMR CNRS 5510, INSA-Lyon, 69621 Villeurbanne, France;* orcid.org/0000-0003-1952-2602

Complete contact information is available at: https://pubs.acs.org/10.1021/acsomega.5c09586

Notes

The authors declare no competing financial interest.

ACKNOWLEDGMENTS

Y.G. gratefully acknowledges funding from the JST FOREST, Grant No. JPMJFR205D, and the Mitsubishi Foundation Research Grants in the Natural Sciences. The authors are also grateful to FRIS-CoRE, a shared facilities environment, where part of this research was conducted.

REFERENCES

(1) Asaka, K.; Okuzaki, H. *Soft Actuators: Materials, Modeling, Applications, and Future Perspectives*; Springer Nature, 2019.

(2) Tan, M. W. M.; Wang, H.; Gao, D.; Huang, P.; Lee, P. S. Towards high performance and durable soft tactile actuators. *Chem. Soc. Rev.* **2024**, *53*, 3485−3535, DOI: 10.1039/D3CS01017A.

(3) Shintake, J.; Cacucciolo, V.; Shea, H.; Floreano, D. Soft biomimetic fish robot made of dielectric elastomer actuators. *Soft Rob.* **2018**, *5*, 466−474.

(4) Ji, X.; Liu, X.; Cacucciolo, V.; Civet, Y.; El Haitami, A.; Cantin, S.; Perriard, Y.; Shea, H. Untethered feel-through haptics using 18-μm thick dielectric elastomer actuators. *Adv. Funct. Mater.* **2021**, *31*, No. 2006639.

(5) Benouhiba, A.; Holzer, S.; Konstantinidi, S.; Civet, Y.; Perriard, Y. The elastic frontier: dielectric elastomer actuators in healthcare technology. *Smart Mater. Struct.* **2025**, *34*, No. 033001.

(6) Tang, C.; Du, B.; Jiang, S.; Wang, Z.; Liu, X.-J.; Zhao, H. A review on high-frequency dielectric elastomer actuators: materials, dynamics, and applications. *Adva. Intell. Syst.* **2024**, *6*, No. 2300047.

(7) Wang, Y.; Ma, X.; Jiang, Y.; Zang, W.; Cao, P.; Tian, M.; Ning, N.; Zhang, L. Dielectric elastomer actuators for artificial muscles: A comprehensive review of soft robot explorations. *Resour. Chem. Mater.* **2022**, *1*, 308−324.

(8) Coativy, G.; Yuse, K.; Diguet, G.; Perrin, V.; Seveyrat, L.; Dalmas, F.; Livi, S.; Courbon, J.; Takana, H.; Cavaillé, J. Role of charge carriers in long-term kinetics of polyurethane electroactuation. *Smart Mater. Struct.* **2022**, *31*, No. 125019.

(9) Hashimoto, N.; Shigemune, H.; Minaminosono, A.; Maeda, S.; Sawada, H. Self-Assembled 3D Actuator Using the Resilience of an Elastomeric Material. *Front. Rob. AI* **2020**, *6*, No. 152.

(10) Shimizu, K.; Nagai, T.; Shintake, J. Dielectric elastomer fiber actuators with aqueous electrode. *Polymers* **2021**, *13*, No. 4310.

(11) Haghiashtiani, G.; Habtour, E.; Park, S.-H.; Gardea, F.; McAlpine, M. C. 3D printed electrically-driven soft actuators. *Extreme Mech. Lett.* **2018**, *21*, 1−8.

(12) Chortos, A.; Hajiesmaili, E.; Morales, J.; Clarke, D. R.; Lewis, J. A. 3D printing of interdigitated dielectric elastomer actuators. *Adv. Funct. Mater.* **2020**, *30*, No. 1907375.

(13) Yi, J.; Babick, F.; Strobel, C.; Rosset, S.; Ciarella, L.; Borin, D.; Wilson, K.; Anderson, I.; Richter, A.; Henke, E.-F. M. Characterizations and inkjet printing of carbon black electrodes for dielectric elastomer actuators. *ACS Appl. Mater. Interfaces* **2023**, *15*, 41992−42003.

(14) Schlatter, S.; Grasso, G.; Rosset, S.; Shea, H. Inkjet printing of complex soft machines with densely integrated electrostatic actuators. *Adv. Intell. Syst.* **2020**, *2*, No. 2000136.

(15) Canales, A.; Jia, X.; Froriep, U. P.; Koppes, R. A.; Tringides, C. M.; Selvidge, J.; Lu, C.; Hou, C.; Wei, L.; Fink, Y.; Anikeeva, P. Multifunctional fibers for simultaneous optical, electrical and chemical interrogation of neural circuits in vivo. *Nat. Biotechnol.* **2015**, *33*, 277−284.

(16) Park, S.; Guo, Y.; Jia, X.; Choe, H. K.; Grena, B.; Kang, J.; Park, J.; Lu, C.; Canales, A.; Chen, R.; et al. One-step optogenetics with multifunctional flexible polymer fibers. *Nature Neurosci.* **2017**, *20*, 612−619.

(17) Saizaki, T.; Kubo, M.; Sato, Y.; Abe, H.; Ohshiro, T.; Mushiake, H.; Sorin, F.; Guo, Y. The development of aptamer-coupled microelectrode fiber sensors (apta-μFS) for highly selective neurochemical sensing. *Anal. Chem.* **2023**, *95*, 6791−6800.

(18) Wu, J.; Sato, Y.; Guo, Y. Microelectronic fibers for multiplexed sweat sensing. *Anal. Bioanal. Chem.* **2023**, *415*, 4307−4318.

(19) Sato, Y.; Guo, Y. Shape-memory-alloys enabled actuatable fiber sensors via the preform-to-fiber fabrication. *ACS Appl. Eng. Mater.* **2023**, *1*, 822−831.

(20) Choi, J.; Zheng, Q.; Abdelaziz, M. E.; Dysli, T.; Bautista-Salinas, D.; Leber, A.; Jiang, S.; Zhang, J.; Demircali, A. A.; Zhao, J.; et al. Thermally drawn shape and stiffness programmable fibers for medical devices. *Adv. Healthcare Mater.* **2025**, *14*, No. 2403235.

(21) Wan, X.; Chen, S.; Ma, J.; Dong, C.; Banerjee, H.; Laperrousaz, S.; Piveteau, P.-L.; Meng, Y.; Leng, J.; Sorin, F. Multimaterial Shape Memory Polymer Fibers for Advanced Drug Release Applications. *Adv. Fiber Mater.* **2025**, *7*, 1−14.

(22) Lee, Y.; Koehler, F.; Dillon, T.; Loke, G.; Kim, Y.; Marion, J.; Antonini, M.-J.; Garwood, I. C.; Sahasrabudhe, A.; Nagao, K.; et al. Magnetically actuated fiber-based soft robots. *Adv. Mater.* **2023**, *35*, No. 2301916.

(23) Banerjee, H.; Leber, A.; Laperrousaz, S.; La Polla, R.; Dong, C.; Mansour, S.; Wan, X.; Sorin, F. Soft multimaterial magnetic fibers and textiles. *Adv. Mater.* **2023**, *35*, No. 2212202.

(24) Leber, A.; Dong, C.; Laperrousaz, S.; Banerjee, H.; Abdelaziz, M. E.; Bartolomei, N.; Schyrr, B.; Temelkuran, B.; Sorin, F. Highly integrated multi-material fibers for soft robotics. *Adv. Sci.* **2023**, *10*, No. 2204016.

(25) Abdelaziz, M. E. M. K.; Zhao, J.; Rosa, B. G.; Lee, H.-T.; Simon, D.; Vyas, K.; Li, B.; Koguna, H.; Li, Y.; Demircali, A. A.; et al. Fiberbots: Robotic fibers for high-precision minimally invasive surgery. *Sci. Adv.* **2024**, *10*, No. eadj1984.

(26) Watanabe, M.; Kato, T.; Suzuki, M.; Amaike, Y.; Hirai, T. Bending electrostriction in polyurethanes containing ions as contaminants or additives. *Jpn. J. Appl. Phys.* **1999**, *38*, No. L872.
(27) Qian, M.; Wang, X.; Yao, L.; Zhu, Y. Enhanced Mechanical and Dielectric Properties of Polyurethane Elastomers Containing Modified SiO2. *ACS Omega* **2024**, *9*, 47315−47323.
(28) Renard, C.; Wang, D.; Han, P.; Xiong, S.; Wen, Y.; Dang, Z.-M. Remarkably improved electromechanical actuation of polyurethane enabled by blending with silicone rubber. *RSC Adv.* **2017**, *7*, 22900−22908.
(29) Hirai, T.; Sadatoh, H.; Ueda, T.; Kasazaki, T.; Kurita, Y.; Hirai, M.; Hayashi, S. Polyurethane-elastomer-actuator. *Die Angew. Makromol. Chem. Appl. Macromol. Chem. Phys.* **1996**, *240*, 221−229.
(30) Gu, G.-Y.; Zhu, J.; Zhu, L.-M.; Zhu, X. A survey on dielectric elastomer actuators for soft robots. *Bioinspiration Biomimetics* **2017**, *12*, No. 011003.
(31) Watanabe, M.; Yokoyama, M.; Ueda, T.; Kasazaki, T.; Hirai, M.; Hirai, T. Bending deformation of monolayer polyurethane film induced by an electric field. *Chem. Lett.* **1997**, *26*, 773−774.
(32) Watanabe, M.; Hirai, T. Bending-electrostrictive response of polyurethane films subjected to a reversed electric field. *J. Appl. Polym. Sci.* **2004**, *92*, 3644−3650.

https://doi.org/10.1021/acsomega.5c09586
ACS Omega 2026, 11, 5716−5725